Process Dynamics of Distributed Parameter Counterflow Systems in Laminar Flow

RICHARD R. STEWART and DUANE F. BRULEY

Clemson University, Clemson, South Carolina

Many studies dealing with the process dynamics of distributed parameter counterflow systems have been reported in the literature. Nearly all of the investigators have considered counterflow systems whose dynamic performance can be described mathematically by a partial differential equation having only two independent variables. For example, in previous studies of double pipe heat exchanger dynamics (*11, 12*) an accurate mathematical description of the system was obtained with time and axial position as the independent variables. As a result of these and other studies, methods of extracting the theoretical process dynamics from mathematical models of distributed parameter counterflow systems having time and a single space dimension as independent variables are well known.

Several papers dealing with steady state solutions of countercurrent laminar flow problems have been reported. Nunge and Gill (*10*) presented a separation of variables solution for a laminar counterflow double-pipe heat exchanger at steady state. Their solution required a convergent series in both positive and negative eigenvalues in order to satisfy the split boundary conditions. The negative set of eigenvalues occurs because one of the fluid velocities is negative with respect to a fixed coordinate system. The split boundary conditions occur because the axial position boundary conditions are usually known at the fluid inlets which are at opposite ends of the system. The eigenvalues for this steady state case were evaluated numerically using an iterative integration procedure.

In the present study of an unsteady state case, Laplace transformed energy balance equations result which are similar in form to the energy balance equations for the steady state case, for example, Equations (3) and (6) herein. However, these transformed equations for the unsteady state case contain an additional term which includes the Laplace transform variable, s, as a parameter. Because the steady state solution of Nunge and Gill involved a numerical integration step to determine the eigenvalues and because the complex parameter, s, complicates the unsteady state equations, the direct transfer function substitution method (*2, 3*) and the use of a completely numerical solution was chosen for the unsteady state equations.

Completely numerical solutions for the steady state case have been reported, also by Nunge and Gill (*9*). Their numerical procedure was a modification of the work of King (*6*). The present study extends the method of King, as modified by Nunge and Gill, to the unsteady state case.

The present study is concerned with mathematical modeling and theoretical calculation of process dynamics for distributed parameter counterflow systems which require two space variables and time for an accurate mathematical description. Most distributed parameter counterflow heat and mass transfer systems having radially dependent velocity, temperature, and/or concentration profiles fall into this category.

A wetted wall column using air and water in countercurrent laminar flow was selected for study. This system was not chosen for its industrial importance but rather for the following reasons:

1. An air-water system is inexpensive and experimentally convenient.
2. Heat and mass transfer coefficients are available from the existing literature.
3. The system is an example of a distributed parameter counterflow process requiring two space variables and time for an accurate mathematical description.
4. The velocity and temperature profiles for experimental equipment of this design are standard and reproducible. Also, the areas for heat and mass transfer are reasonably well defined.
5. The countercurrent flow system generates a split boundary value problem which is a type frequently encountered in chemical engineering process analysis but often difficult to handle mathematically.

The second and fourth considerations are of particular importance when the objective of the experimental analysis is primarily to validate the theoretical procedure for extracting process dynamic information. Knowledge of the coefficients, profiles, and areas minimizes the difficulties in physical and thermal parameter characterization so that comparisons of theoretical and experimental results essentially test the models and the method of extracting dynamic data.

The problem is solved numerically in the frequency domain. The frequency domain approach was selected to reduce the problem to one in two space dimensions with frequency, ω, as a parameter [Equations (8) and (9)]. A more obvious approach would have been solution of the three-dimensional problem with time, θ, as the third dimension [Equation (2)]. While finite difference procedures for solving the three dimensional problem are well known, trial and error is required at each time increment when these procedures are applied to a laminar counterflow system. The computer time required to solve the three-dimensional problem at the large number of time increments required to obtain the system transient response would be considerably greater than that required to solve the two-dimensional problem at several frequencies.

EXPERIMENTAL APPARATUS AND PROCEDURE

The purpose of this work is to present a theoretical method for extracting the process dynamics of distributed parameter counterflow systems which require a three dimensional partial differential equation for an accurate mathematical description. As a result, the experimental apparatus and procedure which have been described previously (*2,3,8,13,14*) are not discussed at length.

The wetted-wall column test section consisted of a vertical 1 in. I.D. plexiglas tube 18 in. in length. It was surrounded by a 4 in. I.D. plexiglas tube to create an annular space which served as a water jacket to minimize heat loss. The water entered the annulus near the bottom and flowed to the top of the test section before overflowing down the inside wall of the inner tube in the form of a thin film.

The air entered the bottom of the test section after passing through a 1 in. I.D. calming section 4 ft. in length. Figures 1

Richard R. Stewart is at Northeastern University, Boston, Massachusetts.

and 2 show a diagram of the experimental apparatus and a detailed cross section of the wetted wall test section, respectively.

The experimental frequency response of the countercurrent laminar flow system was obtained by the pulse testing method (*4, 8*). Gas phase inlet and outlet thermocouples of copper-constantan construction were mounted on depth micrometers and connected through a preamplifier to a dual channel strip chart recorder. The time constant of each thermocouple was less than 0.04 sec.

Before pulsing the system, steady state operation was attained with air flowing through the line on which a heating tape was located. In addition to supplying heat by means of the heating tape, the nichrome pulser at the base of the calming section was sufficiently energized to maintain a temperature of 123°F. at the test section inlet. The system was pulsed by quickly increasing the powerstat setting and then quickly returning it to its steady state position. Just before the desired pulse amplitude was reached, the handle connecting the two stopcocks in the parallel air lines was quickly moved to change the air flow from the heated line to the air line which was cooled by dry ice inside a Dewar flask. When the input pulse had closed to within ½ deg. of the steady state value, the handle was gradually moved back to its original position thereby restoring air flow to the heated air line and re-establishing steady state conditions.

At the laminar flow conditions studied, the air phase Reynolds number was 740 at an inlet temperature of 123°F. and an inlet humidity of 0.002 lb. water vapor/lb. dry air. The water phase Reynolds number (*1*) was 962 at an inlet temperature of 77°F. The amplitude of the air phase temperature pulses ranged from 3 to 5°F. Larger pulses were not used because of the danger of forcing process nonlinearities that would invalidate the linear system pulse testing technique employed.

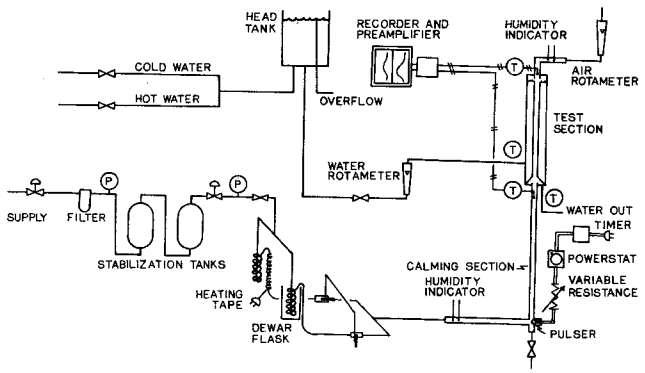

Fig. 1. Diagram of experimental apparatus.

MATHEMATICAL MODELS

Derivation of Models

The laminar flow model is based upon the following assumptions:

1. Axial heat conduction is negligible.
2. At the gas-liquid interface the liquid phase velocity gradient is zero.
3. The mass transfer heat effects are negligible.
4. Heat loss from the liquid phase to the surroundings is negligible.
5. Physical and transport properties are constant.
6. Viscous dissipation is negligible.

Assumption 2 implies that the liquid velocity profile is not affected by the presence of the gas phase and vice versa. Distortion of both profiles near the interface is therefore neglected.

In the derivation which follows, Equations (1) to (3) and (6) to (12) contain no subscripts since these equations apply equally to both phases. Any equation in this group may be written specifically for either phase by subscripting all variables (except θ) and all constants, (v_m, α, and R), with a g to obtain the gas phase equation and

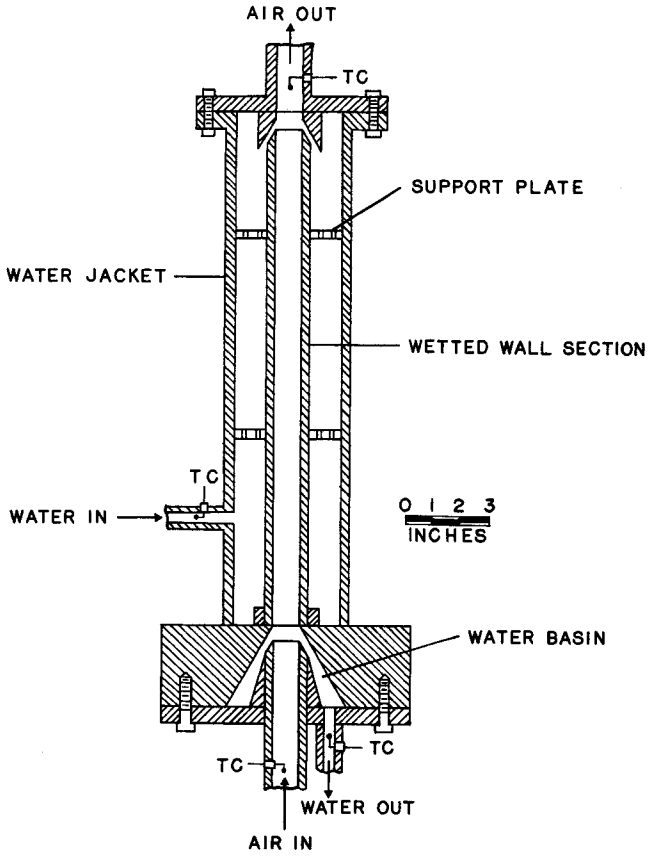

Fig. 2. Detailed cross section of wetted wall column.

with an l to obtain the liquid phase equation.

The following equation is obtained from an energy balance on either the gas or liquid phase:

$$\frac{\partial T}{\partial \theta} + v\frac{\partial T}{\partial z} = \alpha\left(\frac{1}{r}\frac{\partial T}{\partial r} + \frac{\partial^2 T}{\partial r^2}\right) \tag{1}$$

The dynamic equation is obtained by first expressing the temperature T, as the sum of a steady state and a dynamic component and substituting this sum into Equation (1). When the steady state portion of Equation (1) is subtracted from the combined steady state and dynamic equation the following dynamic equation is obtained:

$$\frac{\partial t}{\partial \theta} + v\frac{\partial t}{\partial z} = \alpha\left(\frac{1}{r}\frac{\partial t}{\partial r} + \frac{\partial^2 t}{\partial r^2}\right) \tag{2}$$

Taking the Laplace transformation of Equation (2) yields:

$$s\bar{t} + v\frac{\partial \bar{t}}{\partial z} = \alpha\left(\frac{1}{r}\frac{\partial \bar{t}}{\partial z} + \frac{\partial^2 \bar{t}}{\partial r^2}\right) \tag{3}$$

Next, the following transfer functions are defined:

$$\frac{\bar{t}_g(s,r,z)}{\bar{t}_{g,\text{in}}} = G_g(s,r,z) \tag{4}$$

$$\frac{\bar{t}_l(s,r,z)}{\bar{t}_{g,\text{in}}} = G_l(s,r,z) \tag{5}$$

Equations (4) and (5) are substituted into Equation (3) to obtain one equation for the gas phase transfer function, G_g, and another for the liquid phase transfer function, G_l.

$$sG + v\frac{\partial G}{\partial z} = \alpha\left(\frac{1}{r}\frac{\partial G}{\partial r} + \frac{\partial^2 G}{\partial r^2}\right) \tag{6}$$

The transfer function, G, may be written as the complex

number

$$G(s, r, z) = P(s, r, z) + iQ(s, r, z) \quad (7)$$

The direct substitution of the transfer function indicated by Equation (7) has been used successfully in the analysis of a wetted wall adiabatic humidifier with laminar air flow (*2, 3*).

Substituting Equation (7) and the parabolic velocity profile equation into Equation (6), letting $s = i\omega$ and separating the resulting equation into real and imaginary parts yields the following equations:

$$\omega Q - v_m \left[1 - \left(\frac{r}{R}\right)^2\right] \frac{\partial P}{\partial z} + \alpha\left(\frac{1}{r}\frac{\partial P}{\partial r} + \frac{\partial^2 P}{\partial r^2}\right) = 0 \quad (8)$$

$$-\omega P - v_m \left[1 - \left(\frac{r}{R}\right)^2\right] \frac{\partial Q}{\partial z} + \alpha\left(\frac{1}{r}\frac{\partial Q}{\partial r} + \frac{\partial^2 Q}{\partial r^2}\right) = 0 \quad (9)$$

Substitution of $i\omega$ for s, in stable, linear equations, permits the frequency response corresponding to the system transfer function, G, to be evaluated. In this case the system frequency response is defined with respect to the centerline inlet temperature, $\bar{t}_{g,\text{in}}$.

The variable distances r_g and r_l and fixed distances R_g and R_l are defined by Figure 3. Note that r_l is zero at the gas-liquid interface and that R_l is simply the liquid film thickness.

In order to place the equations in dimensionless form, the following dimensionless variables are defined:

$$\lambda = \frac{\omega z}{v_m} \quad (10)$$

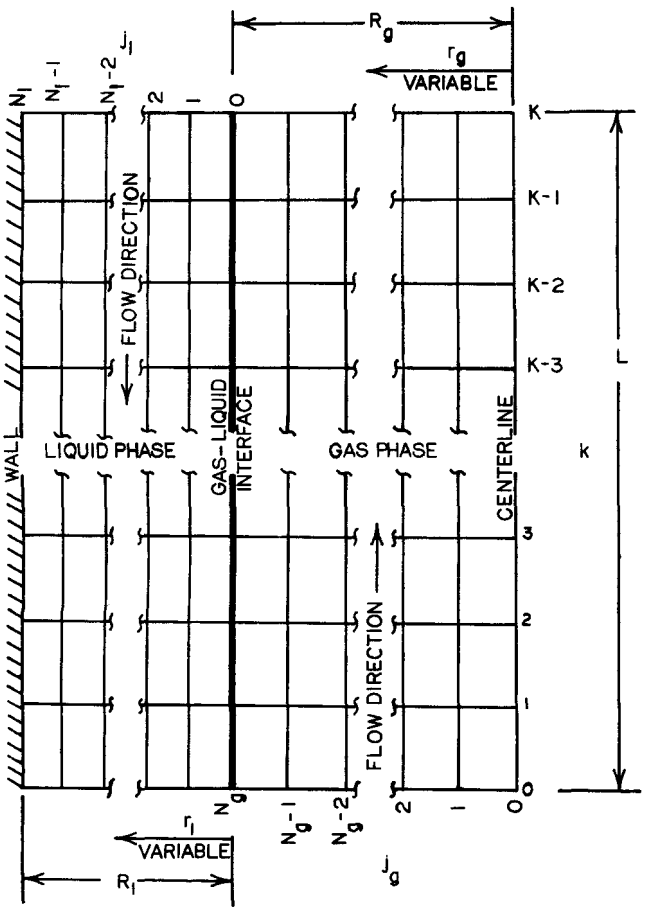

Fig. 3. Mesh model for the numerical solution.

$$D = \frac{\alpha}{\omega R^2} \quad (11)$$

$$\rho = \frac{r}{R} \quad (12)$$

Substitution of Equations (10), (11), and (12) into Equations (8) and (9) yields the following equations for the gas and liquid phases:

Gas phase (g subscripts omitted)

$$Q - (1-\rho^2)\frac{\partial P}{\partial \lambda} + D\left(\frac{1}{\rho}\frac{\partial P}{\partial \rho} + \frac{\partial^2 P}{\partial \rho^2}\right) = 0 \quad (13)$$

$$-P - (1-\rho^2)\frac{\partial Q}{\partial \lambda} + D\left(\frac{1}{\rho}\frac{\partial Q}{\partial \rho} + \frac{\partial^2 Q}{\partial \rho^2}\right) = 0 \quad (14)$$

Liquid phase (l subscripts omitted)

$$Q - (1-\rho^2)\frac{\partial P}{\partial \lambda} + D\left\{\frac{1}{[(R_g/R) + \rho]}\frac{\partial P}{\partial \rho} + \frac{\partial^2 P}{\partial \rho^2}\right\} = 0 \quad (15)$$

$$-P - (1-\rho^2)\frac{\partial Q}{\partial \lambda} + D\left\{\frac{1}{[(R_g/R) + \rho]}\frac{\partial Q}{\partial \rho} + \frac{\partial^2 Q}{\partial \rho^2}\right\} = 0 \quad (16)$$

The form of the liquid phase radial conduction term differs from that of the gas-phase because the liquid phase equations apply over a radial distance which begins at the radius of the gas phase, R_g, rather than at $r = 0$.

Boundary Conditions

Equations (13) through (16) were solved subject to the following boundary conditions:

Gas phase boundary conditions (g subscripts omitted)

boundary condition 1.

$$P(\rho, 0) = \text{determined experimentally}$$

boundary condition 2.

$$Q(\rho, 0) = \text{determined experimentally}$$

boundary condition 3. $\dfrac{\partial P}{\partial \rho}(0, \lambda) = 0$

boundary condition 4. $\dfrac{\partial Q}{\partial \rho}(0, \lambda) = 0$

Liquid phase boundary conditions (l subscripts omitted)

boundary condition 5. $P\left(\rho, \dfrac{\omega L}{v_m}\right) = 0$

boundary condition 6. $Q\left(\rho, \dfrac{\omega L}{v_m}\right) = 0$

boundary condition 7. $\dfrac{\partial P}{\partial \rho}(1, \lambda) = 0$

boundary condition 8. $\dfrac{\partial Q}{\partial \rho}(1, \lambda) = 0$

Gas-liquid interface boundary conditions

boundary condition 9. $P_g(1, \lambda_g) = P_l(0, \lambda_l)$

boundary condition 10. $Q_g(1, \lambda_g) = Q_l(0, \lambda_l)$

boundary condition 11.

$$\left[\frac{k}{R}\frac{\partial P}{\partial \rho}(1, \lambda)\right]_g = \left[\frac{k}{R}\frac{\partial P}{\partial \rho}(0, \lambda)\right]_l$$

boundary condition 12.

$$\left[\frac{k}{R}\frac{\partial Q}{\partial \rho}(1,\lambda)\right]_g = \left[\frac{k}{R}\frac{\partial Q}{\partial \rho}(0,\lambda)\right]_l$$

Gas phase boundary conditions 1 and 2 were determined experimentally using harmonic forcing (2, 3). In order to do this the temperature of the entering air stream was varied in a sinusoidal manner. The resulting sinusoidal temperature variations were measured simultaneously at the centerline and at one other radial position. From the two curves, the experimental inlet amplitude ratio and phase shift relative to the centerline were determined. Knowing the amplitude ratio and phase shift, the corresponding P and Q values were calculated for the radial position in question. Runs were made at several frequencies and radial positions in order to determine the effect of these variables on P and Q. P and Q varied significantly with radial position but were nearly independent of frequency at a given radial position for the frequency range studied. As a result, the same set of radially dependent P and Q data was used as boundary condition 1 and 2 for all frequencies studied.

Boundary conditions 3 and 4 imply radial symmetry of the unsteady state gas phase temperature profile.

Liquid phase boundary conditions 5 and 6 state that the dynamic liquid phase temperature equals zero at the axial position corresponding to the liquid phase inlet. Boundary conditions 7 and 8 include the assumption of no heat loss from the system.

Gas-liquid interface boundary conditions 9 and 10 imply the continuity of the unsteady state temperature profile at the interface. Boundary conditions 11 and 12 equate the unsteady state gas and liquid heat conduction fluxes at the interface.

Systems of Simultaneous Equations

The Crank-Nicholson six-point implicit differencing technique (5, 7) was used to difference the derivatives with respect to radial position. The following four systems of simultaneous equations were derived after finite differencing Equations (13), (14), (15), and (16) and including boundary conditions at the centerline, gas-liquid interface and the wall. The gas and liquid phase subscripts g and l are omitted. The constants A, B, C, E, and F which appear in the equations below are given in the Notation section.

The Gas Phase P Equation, Equation (13)

$$A_0P_{k+1,0} + B_0P_{k+1,1} = F_0P_{k,0} - B_0P_{k,1} - Q_{k,0} \quad (17)$$

Equation (17) applied at the radial mesh point $j_g = 0$.

$$C_jP_{k+1,j-1} + A_jP_{k+1,j} + B_jP_{k+1,j+1} = C_jP_{k,j-1} + E_jP_{j,k} - B_jP_{k,j+1} - Q_{k,j} \quad (18)$$

Equation (18) applies at the radial mesh points $1 \leq j_g \leq N_g - 2$.

$$C_{N-1}P_{k+1,N-2} + A_{N-1}P_{k+1,N-1} = -C_{N-1}P_{k,N-2} + E_{N-1}P_{k,N-1} - B_{N-1}(P_{k,N} + P_{k+1,N}) - Q_{k,N-1} \quad (19)$$

Equation (19) applies at the radial mesh point $j_g = N_g - 1$.

The Gas Phase Q Equation, Equation (14). This system of equations is obtained from Equations (17), (18), and (19) by replacing P by Q and minus Q by P.

The Liquid Phase P Equation, Equation (16)

$$A_1P_{k+1,1} + B_1P_{k+1,2} = -C_1(P_{k,0} + P_{k+1,0}) + E_1P_{k,1} - B_1P_{k,2} - Q_{k,1} \quad (20)$$

Equation (20) applies at the radial mesh points $j_l = 1$.

$$C_jP_{k+1,j-1} + A_jP_{k+1,j} + B_jP_{k+1} = -C_jP_{k,j-1} + E_jP_{k,j} - B_jP_{k,j+1} - Q_{k,j} \quad (21)$$

Equation (21) applies at the radial mesh points $2 \leq j_l \leq N_l - 1$.

$$C_NP_{k+1,N-1} + A_NP_{k+1,N} = A_NP_{k,N-1} + C_NP_{k,N} - Q_{k,N} \quad (22)$$

Equation (22) applies at the radial mesh point $j_l = N_l$.

The Liquid phase Q Equation, Equation (16). This system of equations is obtained from Equations (20), (21), and (22) by replacing P by Q and minus Q by P.

Each of the above four systems of equations can be compactly written in matrix form. Letting the letter H represent the right-hand side of the individual equations and dropping the k and $k+1$ subscripts the equations for the real part of the gas phase transfer function, P_g, [Equations (17), (18), and (19)] may be written as

$$\begin{bmatrix} A_0 & B_0 & & & & \\ C_1 & A_1 & B_1 & & & \\ & - & - & - & & \\ & & - & - & - & \\ & & C_{N-2} & A_{N-2} & B_{N-2} & \\ & & & C_{N-1} & A_{N-1} & \end{bmatrix} \begin{bmatrix} P_0 \\ P_1 \\ - \\ - \\ P_{N-2} \\ P_{N-1} \end{bmatrix} = \begin{bmatrix} H_0 \\ H_1 \\ - \\ - \\ H_{N-2} \\ H_{N-1} \end{bmatrix} \quad (23)$$

The matrix equation for Q_g has the identical tridiagonal coefficient matrix and may be written just as Equation (23) except that the P column matrix is replaced by a Q column matrix. Of course, the elements of the H column matrices will be different for the P_g and Q_g matrix equations.

The equations for the real part of the liquid phase transfer function, P_l, [Equations (20), (21), and (22)] may be written as:

$$\begin{bmatrix} A_1 & B_1 & & & & \\ C_2 & A_2 & B_2 & & & \\ & - & - & - & & \\ & & - & - & - & \\ & & C_{N-1} & A_{N-1} & B_{N-1} & \\ & & & C_N & A_N & \end{bmatrix} \begin{bmatrix} P_1 \\ P_2 \\ - \\ - \\ P_{N-1} \\ P_N \end{bmatrix} = \begin{bmatrix} H_1 \\ H_2 \\ - \\ - \\ H_{N-1} \\ H_N \end{bmatrix} \quad (24)$$

As before, the matrix equation for Q_l has the identical tridiagonal coefficient matrix and may be written just as Equation (24) except that the P column matrix is replaced by a Q column matrix. Again, the elements of the H column matrices will be different for the P_l and Q_l matrix equations.

METHOD OF SOLUTION

A CDC-RPC-4000 digital computer was used to carry out the necessary calculations. Figure 3 shows the locations of the radial and axial mesh points referred to in the following solution steps.

1. Select the frequency, ω, at which amplitude ratio and phase shift data are desired.
2. Based upon the chosen flow rates, fluid properties, and mesh size, calculate each element of the gas and liquid phase tridiagonal coefficient matrices.
3. From experimentally determined input data based upon a centerline amplitude ratio of 1 and phase shift of zero, determine a value of P and Q for each gas phase mesh point ($j_g = 0, 1, \ldots, N_g - 2, N_g - 1$) in the row $k = 0$.
4. At the radial position $j_g = N_g$, the gas-liquid interface, assume values of P and Q for each axial mesh point ($k = 0, 1, \ldots, K - 1, K$).

5. Using the gas phase coefficients determined in step 2 and the most recently determined row of P and Q values, calculate the right-hand side of the N_g equations involving P_g and the N_g equations involving Q_g. This step determines the elements of the H column matrix for the systems of equations involving P_g and Q_g.

6. At this point, the elements of the gas phase tridiagonal coefficient matrix and the elements which constitute the right-hand side of the matrix equations for P_g and Q_g are known. Using the algorithm due to Thomas (7), calculate the values of P_g and Q_g at each radial mesh point in the next axial row.

7. Repeat steps 5 and 6 until the values of P_g and Q_g have been determined at every gas phase mesh point. Note that the gas phase equations are solved by marching the calculation up the column in the direction of gas flow from axial position $k = 0$ to $k = K$.

8. Next, the values of P and Q are determined for the liquid phase. At the axial row $k = K$, the row at which the liquid phase enters the system, let P_l and Q_l equal zero at each radial mesh point ($j_l = 1, 2, \ldots, N_l - 1, N_l$).

9. Using the same axial interface P and Q values chosen in step 4, repeat the liquid phase equivalent of steps 5 to 7. Upon completion of this step, values of P_l and Q_l have been determined at every liquid phase mesh point. Note that the liquid phase equations are solved by marching the calculation down the column in the direction of liquid flow from axial position $k = K$ to $k = 0$.

10. Thus far, a value of P and Q has been determined at every gas and liquid phase mesh point. Note that the axial P and Q interface distributions which were assumed in step 4 were used in both the gas and liquid phase solutions, thereby satisfying boundary conditions 9 and 10. Using the values of P and Q at the interface, at $j_g = N_g - 1$, and at $j_l = 1$, determine whether or not the differenced form of boundary condition 11 and 12 are satisfied within a specified error at each axial position ($k = 0, 1, \ldots, K - 1, K$).

11. If bundary conditions 11 and 12 were satisfied at each axial position, decrease the mesh size to check convergence. If these conditions were not satisfied at each axial position, go to step 4 and repeat steps 4 to 11 with another interface P and Q distribution. Continue repeating steps 4 to 11 until correct P and Q interface distributions are found.

12. Repeat steps 1 to 11 for as many frequencies, ω, as desired.

DISCUSSION

Numerical Trial and Error Solution

A computer program was written to carry out steps 2 to 10. The computer output for one trial consisted of the values of P_g and Q_g at row $k = K$, and P_l and Q_l at row $k = 0$ as well as the values of P and Q at each axial position for radial positions $j_g = N_g - 1$, for the interface ($j_g = N_g$, or $j_l = 0$), and for $j_l = 1$. In addition, the values of the left and right-hand sides of boundary conditions 11 and 12 and the percent difference between them at each interface mesh point were included in the computer output.

Practically, of course, boundary conditions 11 and 12 can never be satisfied exactly when a numerical solution is employed. It is necessary therefore to specify a maximum allowable percent erorr between the left and right-hand side of boundary conditions 11 and 12. This maximum error may depend strongly upon the relative location of the interface and the radial mesh points at which frequency response data are desired and also upon the physical properties of the two fluids. For example, in the present study, upon forcing inlet air temperature, the water temperature did not change significantly form its steady state value. This is reasonable on the basis of comparative heat capacities and mass flow rates of the air and water. However, it means that, in general, the values of P and Q near the centerline are considerably higher than those at the interface and within the liquid phase. Because of the comparatively low interface P and Q values, the centerline and midpoint P and Q values were accurate through three decimal places when boundary conditions 11 and 12 were satisfied to within about $\pm 100\%$. This was checked at two extreme frequencies of 0.01 and 1.0 rad./sec. by satisfying these interface equations to within about $\pm 10\%$ and observing no improvement in the first three decimal places of the centerline and midpoint values. The midpoint is the radial position half way between the centerline and the gas-liquid interface.

It is important to note that while satisfying boundary conditions 11 and 12 to within $\pm 100\%$ was sufficient to determine the amplitude ratio and phase shift at the gas phase centerline and midpoint, it is not sufficient for determination of these quantities at mesh points near the interface and within the water phase. In addition, for other fluids and flow conditions, satisfying the interface equations to within $\pm 100\%$ will not necessarily determine the centerline and midpoint P and Q values as in the present study.

Interaction of P and Q

The equations for P and Q are coupled as shown by Equations (13) through (22). This means that both a P and a Q interface distribution must be assumed before the numerical solution for either P or Q at the various mesh points can begin. It also means that it is not possible to determine accurately the values of either P or Q at the various mesh points unless accurate interface distributions for both P and Q have been determined.

In the present study it was found that the interaction between the equations for P and Q was slight. For example, at one stage the P interface equation (boundary condition 11) was satisfied to within about $\pm 10\%$ at each interface mesh point while the corresponding Q equation (boundary condition 12) still had a mean error of about $\pm 30\%$. By assuming an improved set of interface Q values the Q interface equation was subsequently satisfied to within $\pm 10\%$ with only a very slight change in the P interface distribution being required to maintain the mean error for the P interface equation within about $\pm 10\%$.

To improve the efficiency of the numerical calculation more sophisticated optimization algorithms can be devised for automatically selecting new interface P and Q distributions based upon the accuracy of past distributions. However, the primary objective of this initial study is to formulate a workable method for extracting theoretical frequency response information from complex distributed parameter systems and therefore the development of a more efficient computation procedure is left as a continuation exercise.

Experimental Results

Experimental frequency response results (Figure 4) were obtained by numerical Fourier transformation of the input and output pulses (4, 8).

Agreement between theoretical and experimental results for the centerline amplitude ratio is very good. The experimental values of midpoint amplitude ratio are greater than those predicted by the mathematical model. This difference has been reported previously and has been attributed to an unsymmetric radial temperature profile in the air phase (3, 8).

Phase shift is due to both heat transfer and pure trans-

port delay. The total phase shift is greater than that for pure transport delay for both the experimental and theoretical cases. For the turbulent-turbulent case (*13, 14*) phase shift as found to be a result of pure transport delay only.

The experimental data points shown in Figure 4 were obtained by averaging the results of four separate pulse tests. At high frequencies these average values scattered less and yielded significantly better agreement with theoretical results than any one pulse test. This averaging technique was used successfully in a related study of the turbulent-turbulent flow case (*13, 14*).

Prevous investigators (*4, 8*) have shown that data point scatter becomes severe when Filon's method (*4*) for data reduction is used and the normalized frequency content of the input pulse falls below about 0.3. This was also observed in the present study although the scatter was less pronounced for the averaged data than for data of any one pulse test.

Because of the experimental pulse testing technique used it was necessary to force the system with temperature pulses of small amplitude so that system nonlinearities would not be disturbed. Because of the small amplitudes and the relative heat capacities and mass flow rates of the air-water system, the system response was similar to that of the adiabatic case (*3*). Therefore, the experimental results do not represent a severe test for the theoretical procedure however they do allow an evaluation of the technique for one set of nonadiabatic operating conditions. A more severe test could be made by using two fluids with nearly equal thermal conductivities and heat capacities flowing at approximately the same mass rates. Clearly, the mathematical models would require inclusion of an axial conduction term for fluids of high thermal conductivity flowing at certain rates. Inclusion of this term would change the form of the equations to the extent that the Crank-Nicholson implicit differencing technique would not be applicable.

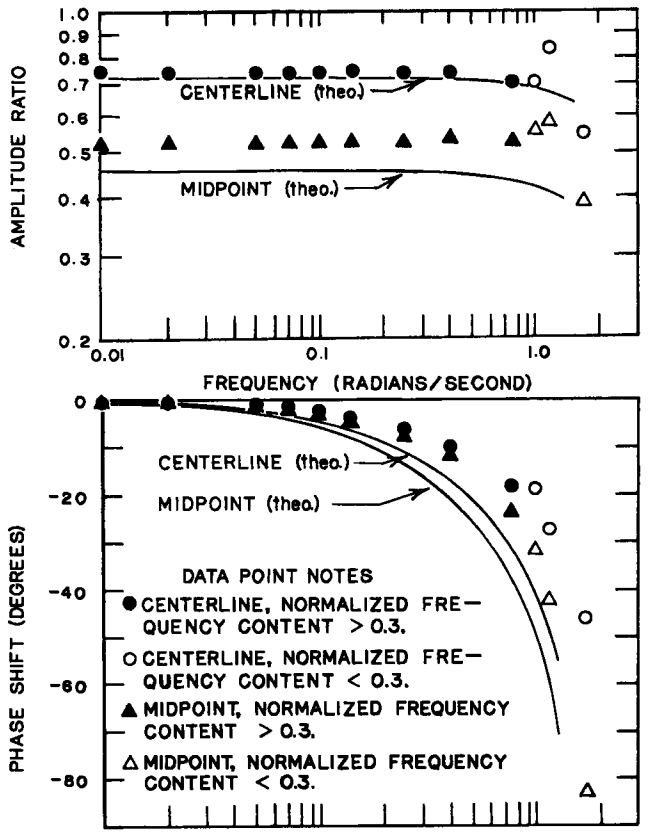

Fig. 4. Comparison of actual and theoretical results.

Another way to obtain better experimental response information to compare with the theoretical results might be by forcing the water-phase rather than the air-phase temperature. However, this would be a difficult procedure when using a wetted-wall column of the design in this experiment since it would be difficult to generate a temperature disturbance that would show up uniformly around the periphery at the inlet to the wetted section. Also the temperature pulse would influence the system response while in the jacket as well as in the column itself. Plans for future experimental testing include the design of a new column that will be suitable for water-phase forcing.

CONCLUSIONS

A method of extracting the theoretical frequency response for distributed parameter counterflow systems whose mathematical description requires two space variables as well as time has been presented. Although the method has been applied to the case of countercurrent flow of two phases in direct contact, it should be possible to extend it to the case wherein the two phases are separated by a solid boundary. Also, the technique should be applicable to systems of more complex geometries than presented here providing the necessary velocity profiles and heat and mass transfer areas can be determined mathematically or experimentally.

In the present study it was necessary to satisfy the interface boundary conditions, boundary conditions 11 and 12, to within only $\pm 100\%$ to determine accurately the centerline and midpoint amplitude ratio and phase shift. This is because the interface and liquid phase temperature changes are quite small compared to the temperature change of the gas phase. The relatively small temperature change of the liquid phase is due to the comparative thermal conductivities, heat capacities, and mass flow rates of the gas and liquid streams.

ACKNOWLEDGMENT

The authors wish to express their gratitude to the Clemson University Computer Center for the use of their facilities. This investigation was supported by the National Science Foundation under Contract No. GP-3027 and by an NDEA fellowship.

NOTATION

D = dimensionless thermal diffusivity
G = transfer function relating gas or liquid temperature changes to a change in the inlet gas temperature
i = $+\sqrt{-1}$
k = thermal conductivity, B.t.u./hr.-sq.ft.-°F./ft.
L = axial length of system, ft.
m = dimensionless radial increment size
n = dimensionless axial increment size
P = real part of transfer function, G
Q = imaginary part of transfer function, G
r = radial position, ft
R_g = radius of gas phase, ft.
R_l = thickness of liquid film, ft.
s = Laplace transform variable
T = temperature, °F.
$\bar{t}$ = Laplace transformed temperature change
v = velocity, ft./hr.
v_m = maximum velocity, ft./hr.
z = axial position, ft.

Greek Letters

α = thermal diffusivity, sq.ft./hr.
ρ = dimensionless radial position

λ = dimensionless axial position
ω = frequency, rad./hr.
θ = time, hr.

Subscripts

g = gas phase
in = gas phase inlet
j = radial mesh point location
k = axial mesh point location
l = liquid phase

Coefficients in Gas Phase Equations (17), (18), (19), and (23)

$$A_0 = -\frac{1}{n} - \frac{2D}{m^2}$$

$$B_0 = \frac{2D}{m^2}$$

$$F_0 = \frac{2D}{m^2} - \frac{1}{n}$$

$$A_j = \frac{1-\rho_j^2}{n} - \frac{D}{m^2} \qquad 1 \leq j_g \leq N_g - 1$$

$$B_j = \frac{D}{2m^2} + \frac{D}{4\rho_j m} \qquad 1 \leq j_g \leq N_g - 1$$

$$C_j = \frac{D}{2m^2} - \frac{D}{4\rho_j m_2} \qquad 1 \leq j_g \leq N_g - 1$$

$$E_j = \frac{D}{m^2} - \frac{1-\rho_j}{n} \qquad 1 \leq j_g \leq N_g - 1$$

Coefficients in Liquid Phase Equations (20), (21), (22), and (24)

$$A_j = -\frac{1-\rho_j^2}{n} - \frac{D}{m^2} \qquad 1 \leq j_l \leq N_l - 1$$

$$B_j = \frac{D}{2m^2} + \frac{D}{4[(R_g/R_l) + \rho_j]m} \qquad 1 \leq j_l \leq N_l - 1$$

$$C_j = \frac{D}{2m^2} - \frac{D}{4[(R_g/R_l) + \rho_j]m} \qquad 1 \leq j_l \leq N_l - 1$$

$$E_j = \frac{D}{m^2} - \frac{1-\rho_j^2}{n} \qquad 1 \leq j_l \leq N_l - 1$$

$$A_N = -\frac{D}{m^2}$$

$$C_N = \frac{D}{m^2}$$

$$E_N = \frac{D}{m^2} - \frac{1-\rho_j^2}{n}$$

LITERATURE CITED

1. Bird, R. B., W. E. Stewart, and E. N. Lightfoot, "Transport Phenomena," p. 41, John Wiley, New York (1962).
2. Bruley, D. F., Ph.D. thesis, Univ. Tennessee, Knoxville, (1962).
3. ——— and J. W. Prados, *AIChE J.*, **10**, 612 (1964).
4. Clements, W. C., Jr., and K. B. Schnelle, Jr., *Ind. Eng. Chem. Proc. Des. Dev.* **2**, 94 (1963).
5. Crank, J., and P. Nicholson, *Proc. Camb. Phil. Soc.*, **43**, 50 (1947).
6. King, C. J., *Lawrence Radiation Lab., Rept UCRL-11196,* Univ. Calif., Berkeley, (Jan. 1964).
7. Lapidus, L., "Digital Computation for Chemical Engineers," p. 254, McGraw-Hill, New York (1962).
8. Lewis, C. I., Bruley, D. F., and D. H. Hunt, *Ind. Eng. Chem. Proc. Des. Dev.*, **6**, 281, (July, 1967).
9. Nunge, R. J., and W. N. Gill, *Int. J. Heat Mass Transfer,* **8**, 873 (1965).
10. ————, *AIChE J.*, **12**, 279 (1966).
11. Stermole, F. J., and M. A. Larson, *ibid.*, **10**, 688 (1964).
12. ————, *Ind. Eng. Chem. Fundamentals,* **2**, 62 (1963).
13. Stewart, R. R., Ph.D. thesis, Clemson Univ., S.C. (1966).
14. Stewart, R. R., and D. F. Bruley, *AIChE J.*, **13**, 793 (1967).

Manuscript received January 24, 1967; revision received April 22, 1968; paper accepted April 25, 1968.

Mass Transfer Limitations in a Trickle-Bed Reactor

CHARLES N. SATTERFIELD, A. A. PELOSSOF, and THOMAS K. SHERWOOD

Massachusetts Institute of Technology, Cambridge, Massachusetts

The hydrogenation of alpha-methylstyrene to cumene at 20 to 50°C. was studied experimentally with a trickle-bed reactor comprising a single vertical column of spherical porous palladium-on-alumina catalyst pellets. Other studies with powdered catalyst and studies in which catalyst pellets were swirled in a reactor allowed the intrinsic kinetics and effectiveness factor of the catalyst pellets to be determined. At 50°C. the reaction rate in the trickle-bed was about one-half of that in the absence of mass transfer limitations in the outside liquid film. The effectiveness factor of the pellets alone at 50°C. was 0.0057, and the tortuosity factor was 7.5. Experimental results are compared with four theoretical models for trickle-bed reactors and criteria are presented for estimating whether mass transfer through the outside film is a significant resistance in an industrial trickle-bed reactor.

A trickle-bed reactor consists of a fixed catalyst bed in which the liquid reactant flows over the catalyst pellets while the reacting gas, which fills the voids, flows either in the same or opposite direction. The rate-controlling step can be one or a combination of the following processes: (a) mass transfer of reactants and/or products between the bulk gas phase and the liquid-gas interface, (b) mass transfer through the liquid film surrounding the pellets, (c) diffusion and simultaneous reaction within the liquid-filled catalyst pores, and (d) intrinsic kinetics of reaction at the catalyst surface. The object of this study was to determine the role played in the performance of a trickle-